CTPU-16-40

Leptonic mono-top from single stop production at LHC

Guang Hua Duan[1], Ken-ichi Hikasa[2], Lei Wu[3,4], Jin Min Yang[1,2], and Mengchao Zhang[5]

[1] *CAS Key Laboratory of Theoretical Physics, Institute of Theoretical Physics, Chinese Academy of Sciences, Beijing 100190, China*

[2] *Department of Physics, Tohoku University, Sendai 980-8578, Japan*

[3] *ARC Centre of Excellence for Particle Physics at the Terascale, School of Physics, The University of Sydney, NSW 2006, Australia*

[4] *Department of Physics and Institute of Theoretical Physics, Nanjing Normal University, Nanjing, Jiangsu 210023, China*

[5] *Center for Theoretical Physics and Universe, Institute for Basic Science (IBS), Daejeon 34051, Korea.*

Abstract

Top squark (stop) can be produced via QCD interaction but also the electroweak interaction at the LHC. In this paper, we investigate the observability of the associated production of stop and chargino, $pp \to \tilde{t}_1\tilde{\chi}_1^-$, in compressed electroweakino scenario at the 14 TeV LHC. Due to the small mass-splitting between the lightest neutralino ($\tilde{\chi}_1^0$) and chargino ($\tilde{\chi}_1^-$), such a single stop production can give a mono-top signature through the stop decay $\tilde{t}_1 \to t\tilde{\chi}_1^0$. Focusing on the leptonic mono-top channel, we propose a lab-frame observable $\cos\theta_{b\ell}$ to reduce the SM backgrounds in virtue of a boosted top quark from the stop decay. We find that the single stop production can be probed at 2σ level at the HL-LHC for $m_{\tilde{t}_1} < 760$ GeV and $m_{\tilde{\chi}_1^0} < 150$ GeV.

PACS numbers:

I. INTRODUCTION

After the discovery of a Higgs boson in 2012 [1, 2], the fundamental mechanism for stabilizing the electroweak scale has become an urgent topic. Weak scale supersymmetry (SUSY) is one of the most promising candidates for addressing such an outstanding theoretical issue. SUSY predicts a plethora of supersymmetric particles, among which the top-squarks (stops) play an important role in cancelling the quadratic divergence in the Higgs boson mass. Naturalness (absence of fine-tuning in the Higgs boson mass) requires stop masses to be below 1 TeV in the MSSM [3]. Therefore, the search for light stops is a sensitive probe of the naturalness in SUSY [4–23].

So far, ATLAS and CMS collaborations have performed extensive searches for stops at the LHC Run-1 and Run-2. Based on a recent Run-2 (~ 15 fb^{-1}) dataset, the stop mass has been excluded up to ~ 1 TeV in simplified models [24–31]. The current search strategies are specialized for different kinematical regions. For example, when $m_{\tilde{t}_1} \gg m_{\tilde{\chi}_1^0} + m_t$, the top quarks from stop decays are usually energetic and can be discriminated from the $t\bar{t}$ background by using endpoint observables, such as M_{T2} [32, 33]. But in the compressed region like $m_{\tilde{t}_1} \approx m_{\tilde{\chi}_1^0} + m_t$, the decay products of the stop are usually too soft to tag and hence the monojet signature is used [34–39].

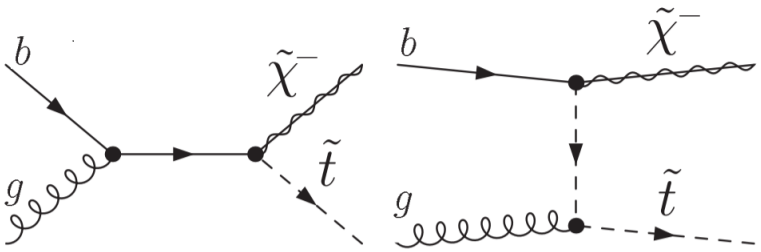

FIG. 1: Feynman diagrams for the associated production of the stop and chargino at the LHC.

Like the top quark, stops can be produced in pair, but also can be singly produced via the electroweak interaction, such as the associated production with a chargino, $bg \to \tilde{t}_1\tilde{\chi}_1^-$ [40–42], as shown in Fig. 1. Such a single stop production can have a sizable cross section at the LHC when the stop and chargino are not heavy or the chargino is much lighter than the stop [40]. Although it may not be a good discovery channel as the stop pair production, its study is meaningful because it can be used as a complementary channel to probe the electroweak properties of the stop [41, 42].

In this work, we explore the feasibility of probing the single stop production process $pp \to \tilde{t}_1(\to t\tilde{\chi}_1^0)\tilde{\chi}_1^- + X$ in a compressed SUSY scenario, where the chargino $\tilde{\chi}_1^\pm$ is almost degenerate with the lightest neutralino $\tilde{\chi}_1^0$. Such a spectrum is motivated by natural SUSY [4, 5] or the well-tempered neutralino frameworks [43]. Due to the small mass splitting between $\tilde{\chi}_1^\pm$ and $\tilde{\chi}_1^0$, such a single stop production will give the mono-top signature [42, 44–48] and in Ref. [42] its full-hadronic final states with top tagging technique are studied. In this study, we focus on the leptonic decay channel of the top quark, which will have a moderate background (no QCD backgrounds) and the cut on the leptonic m_T can greatly reduce the $t\bar{t}$ and $W + b$ backgrounds [46, 47]. We also investigate the open angle of the charged lepton and b-jet in the top decay in lab-frame and find such an observable can effectively reduce the SM backgrounds of the single stop production.

This work is organized as follows. In Sec. II, we present the single stop production and stop decays in the compressed electroweakino scenario. In Sec. III, we perform detailed Monte Carlo simulations for the leptonic mono-top signature from the single stop production. Finally, we summarize our conclusions in Sec. IV.

II. SINGLE PRODUCTION AND DECAYS OF STOP IN COMPRESSED ELECTROWEAKINO SCENARIO

In the MSSM, the stop mass matrix in the gauge-eigenstate basis ($\tilde{t}_L$,$\tilde{t}_R$) is given by

$$M_{\tilde{t}}^2 = \begin{pmatrix} m_{\tilde{t}_L}^2 & m_t X_t^\dagger \\ m_t X_t & m_{\tilde{t}_R}^2 \end{pmatrix} \tag{1}$$

with

$$m_{\tilde{t}_L}^2 = m_{\tilde{Q}_{3L}}^2 + m_t^2 + m_Z^2 \left(\frac{1}{2} - \frac{2}{3}\sin^2\theta_W\right)\cos 2\beta, \tag{2}$$

$$m_{\tilde{t}_R}^2 = m_{\tilde{U}_{3R}}^2 + m_t^2 + \frac{2}{3} m_Z^2 \sin^2\theta_W \cos 2\beta, \tag{3}$$

$$X_t = A_t - \mu \cot\beta. \tag{4}$$

Here $m_{\tilde{Q}_{3L}}$ and $m_{\tilde{U}_{3R}}$ are the soft-breaking mass parameters for the third generation left-handed squark doublet $\tilde{Q}_{3L}$ and the right-handed stop $\tilde{U}_{3R}$, respectively. A_t is the stop soft-breaking trilinear parameter. We have neglected the generation mixing here. This

hermitian matrix can be diagonalized by a unitary transformation:

$$\begin{pmatrix} \tilde{t}_1 \\ \tilde{t}_2 \end{pmatrix} = \begin{pmatrix} \cos\theta_{\tilde{t}} & \sin\theta_{\tilde{t}} \\ -\sin\theta_{\tilde{t}} & \cos\theta_{\tilde{t}} \end{pmatrix} \begin{pmatrix} \tilde{t}_L \\ \tilde{t}_R \end{pmatrix}, \tag{5}$$

where $\theta_{\tilde{t}}$ is the mixing angle between left-handed ($\tilde{t}_L$) and right-handed ($\tilde{t}_R$) stops. In the mass eigenstates, the relevant interactions of the stop and electroweakinos are given by

$$\mathcal{L}_{\tilde{t}_1 \bar{b} \tilde{\chi}_i^+} = \tilde{t}_1 \bar{b} (f_L^C P_L + f_R^C P_R) \tilde{\chi}_i^+ + h.c. \,, \tag{6}$$

$$\mathcal{L}_{\tilde{t}_1 \bar{t} \tilde{\chi}_i^0} = \tilde{t}_1 \bar{t} (f_L^N P_L + f_R^N P_R) \tilde{\chi}_i^0 + h.c. \,, \tag{7}$$

where $P_{L/R} = (1 \mp \gamma_5)/2$, and

$$f_L^N = -\left[\frac{g_2}{\sqrt{2}} N_{i2} + \frac{g_1}{3\sqrt{2}} N_{i1}\right] \cos\theta_{\tilde{t}} - y_t N_{i4} \sin\theta_{\tilde{t}} \tag{8}$$

$$f_R^N = \frac{2\sqrt{2}}{3} g_1 N_{i1}^* \sin\theta_{\tilde{t}} - y_t N_{i4}^* \cos\theta_{\tilde{t}}, \tag{9}$$

$$f_L^C = y_b U_{i2}^* \cos\theta_{\tilde{t}}, \tag{10}$$

$$f_R^C = -g_2 V_{i1} \cos\theta_{\tilde{t}} + y_t V_{i2} \sin\theta_{\tilde{t}}, \tag{11}$$

with $y_t = \sqrt{2} m_t/(v \sin\beta)$ and $y_b = \sqrt{2} m_b/(v \cos\beta)$ being the top and bottom Yukawa couplings, respectively. When $\tan\beta$ is large, the values of y_b can be sizable. The neutralino and chargino mixing matrices N_{ij}, U_{ij}, V_{ij} are defined in [49]. The compressed electroweakino spectrum, $m_{\tilde{\chi}_1^\pm} - m_{\tilde{\chi}_1^0} \ll m_{\tilde{\chi}_1^0}$, can be realized in two limits:

(i) $\mu \ll M_{1,2}$, $V_{11}, U_{11}, N_{11,12,21,22} \sim 0$, $V_{12} \sim \mathrm{sgn}(\mu)$, $U_{12} \sim 1$ and $N_{13,14,23} = -N_{24} \sim 1/\sqrt{2}$. In this limit, the two neutralinos $\tilde{\chi}_{1,2}^0$ and the chargino $\tilde{\chi}_1^\pm$ are nearly degenerate higgsinos ($\tilde{H}^\pm$). Such a higgsino LSP scenario may be probed at the high luminosity LHC [50–54].

(ii) $M_2 \ll \mu, M_1$, $V_{11}, U_{11} \sim 1$, $V_{12}, U_{12} \sim 0$, $N_{11,13,14}$, $N_{22,23,24} \sim 0$, and $N_{12,21} \sim 1$. In this case, the lightest neutralino $\tilde{\chi}_1^0$ and the lighter chargino $\tilde{\chi}_1^\pm$ are nearly degenerate winos ($\tilde{W}^\pm$). If the small splitting between $\tilde{\chi}_1^\pm$ and $\tilde{\chi}_1^0$ is not too small, the mono-jet with soft photon events can be used to detect this wino LSP scenario at the LHC [55–57].

We evaluate the mass spectrum and branching ratios of all sparticles with SUSY-HIT [59]. We use MadGraph5_aMC@NLO [60] to calculate the leading order cross section of the

single stop production. The NNPDF23LO1 [61] parton distribution functions are chosen for our calculations. The renormalization and factorization scales are taken to be the default value. We include the NLO-QCD effect by applying a K-factor of 1.3 [40, 42] to the single stop production. It should be noted that the single stop production not only relies on the nature of the electroweakinos, but also is affected by the polarized states of the stop. To demonstrate this, we consider two cases: the left-handed stop $\tilde{t}_L$ by taking $m_{\tilde{U}_{3R}} = 2$ TeV to decouple the right-handed component, and the right-handed stop $\tilde{t}_R$ by taking $m_{\tilde{Q}_{3L}} = 2$ TeV to decouple the left-handed component.

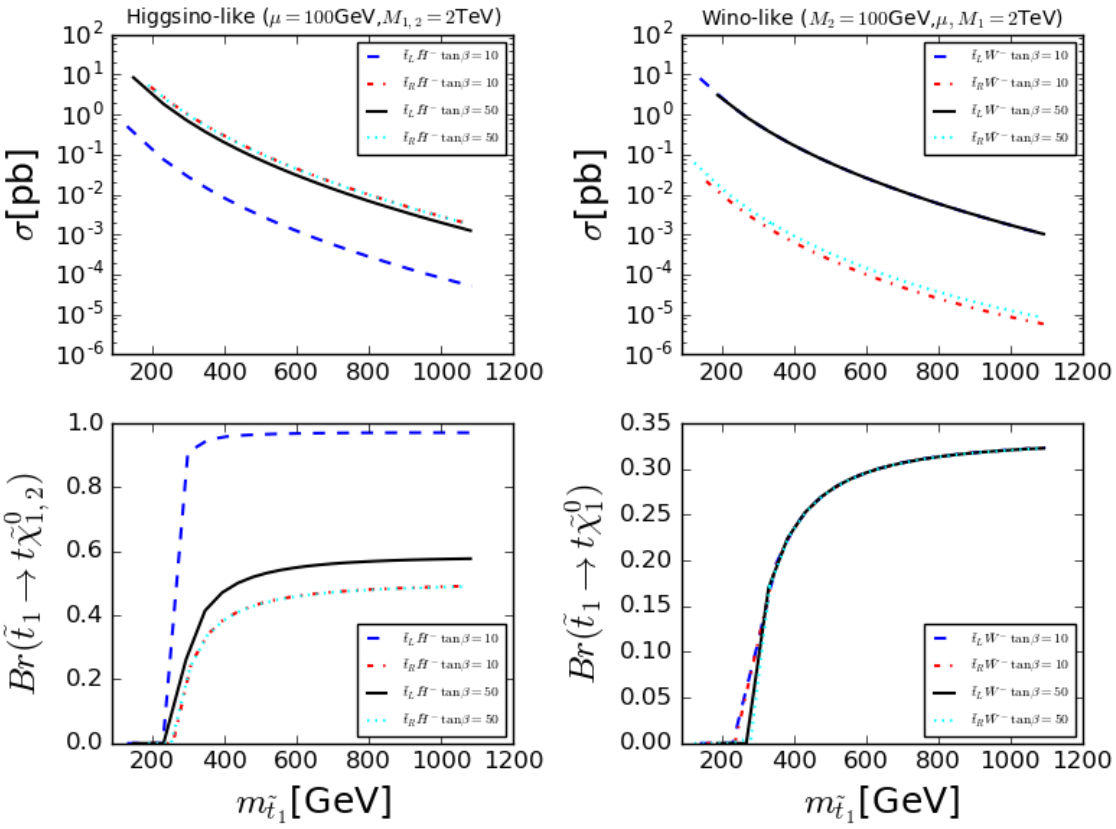

FIG. 2: Cross sections of the associated production of stop and chargino at the 14 TeV LHC (*upper panels*), and the stop decay branching ratios (*lower panels*) in two compressed electroweakino scenarios, where $\tan\beta = 10$ and 50. The left (right) two figures are for a higgsino-like (wino-like) chargino $\tilde{\chi}_1^\pm$.

In the upper panels of Fig. 2, we show the cross sections of the associated production of stop and chargino at the 14 TeV LHC for four different final states: $\tilde{t}_L\tilde{H}^-$, $\tilde{t}_R\tilde{H}^-$, $\tilde{t}_L\tilde{W}^-$ and $\tilde{t}_R\tilde{W}^-$. The contributions of the conjugate processes are included. For a higgsino-like

chargino, we can see that the associated production of $\tilde{t}_R\tilde{H}^-$ has the largest cross section, which can reach about 3 pb at $m_{\tilde{t}_1} = 200$ GeV. While the cross section of $\tilde{t}_L\tilde{H}^-$ strongly depends on the value of $\tan\beta$, since the coupling of the left-handed stop with $\tilde{\chi}_1^\pm$ is dominated by the bottom Yukawa coupling y_b and can be enhanced by a large $\tan\beta$. For a wino-like chargino, the cross section of $\tilde{t}_L\tilde{W}^-$ is always much larger than that of $\tilde{t}_R\tilde{W}^-$ because of the gauge interactions. We also plot the branching ratios of stop decaying to the top quark and neutralinos in the lower panels of Fig. 4. For higgsino case, it can be seen that a left-handed stop $\tilde{t}_L$ dominantly decays to $t\tilde{\chi}_{1,2}^0$ at $\tan\beta = 10$. The reason is that the decay width of $b\tilde{\chi}_1^+$ is proportional to y_b and is suppressed for a small $\tan\beta$. If the stop is right-handed $\tilde{t}_R$, its couplings with $\tilde{\chi}_{1,2}^0$ and $\tilde{\chi}_1^\pm$ are proportional to y_t, and the branching ratios of $\tilde{t}_R \to t\tilde{\chi}_{1,2}^0$ and $\tilde{t}_R \to b\tilde{\chi}_1^+$ are about 50% and 50%, respectively. For the wino case, both $\tilde{t}_L$ and $\tilde{t}_R$ decay to $t\tilde{\chi}_1^0$ with the same branching ratio. In the following, we take the higgsino-like chargino and right-handed stop as an example to investigate the observability of the single stop production at the LHC.

III. LEPTONIC MONO-TOP SIGNATURE FROM SINGLE STOP PRODUCTION AT THE LHC

Since $\tilde{\chi}_1^\pm$ and $\tilde{\chi}_{1,2}^0$ are the nearly degenerate higgsinos in our considered scenario, the mass splitting between them is small so that $\tilde{\chi}_1^\pm$ and $\tilde{\chi}_2^0$ appear as missing transverse energy at the LHC. This leads to the mono-top signature for the single stop production at the LHC, which is

$$pp \to \tilde{t}_1(\to t\tilde{\chi}_{1,2}^0)\tilde{\chi}_1^- \to t + \not{E}_T, \tag{12}$$

In our simulation, we focus on the leptonic mono-top channel. Contrary to the hadronic mode, the problematic QCD multijet background can be safely neglected in this case. We use MadGraph5_aMC@NLO [60] to generate the parton level events. Then, we perform the parton shower and hadronization by Pythia [62]. The jets are clustered by the anti-k_t algorithm with a cone radius $\Delta R = 0.4$ [64]. We implement the detector effects with Delphes [63].

The SM backgrounds are dominated by the following three processes:

- The largest SM backgrounds are the semi- and di-leptonic $t\bar{t}$ productions, where the missing lepton and the limited jet energy resolution will lead to relatively large missing

E_T. The leading order cross section of $t\bar{t}$ production is normalized to its approximate next-to-next-to-leading-order value $\sigma_{t\bar{t}}^{\rm NNLOapprox} = 920$ pb [65].

- The subdominant background is the single top production, which is irreducible, up to a jet that could come from ISR. We include three production modes tj, tb and tW in our simulation.

There are other possible SM backgrounds, such as $W + jets$ and the diboson production VV. But for $W + jets$, the mistag rate of a light jet as a b-jet in current ATLAS and CMS analyses is of the order of 10^{-2} and 10^{-3}, depending on the working point of the b-tagging algorithm. The acceptance of this background after cuts is found to be negligibly small. On the other hand, VV backgrounds can also be neglected because of their small cross sections and the difficulty of faking a $b\ell\not{E}_T$ final state in WW, WZ and ZZ backgrounds.

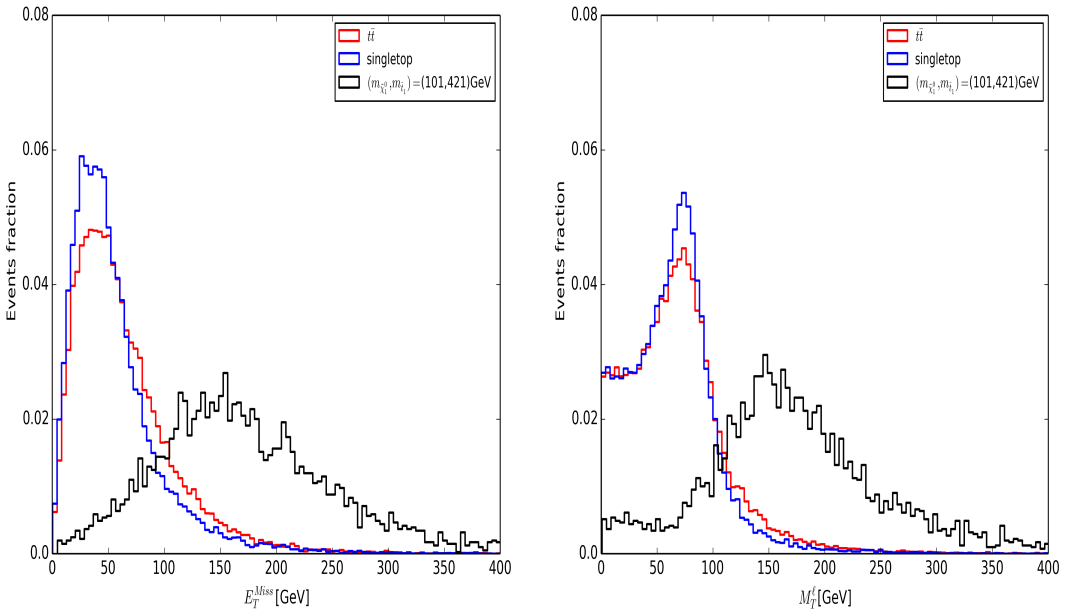

FIG. 3: Distributions of transverse missing energy $\not{E}_T$ and the transverse mass of the lepton plus missing energy system M_T^{ℓ}. The signal benchmark point is for $m_{\tilde{\chi}_1^0} = 101$ GeV and $m_{\tilde{t}_1} = 421$ GeV.

In Fig. 3, we present the distributions of the transverse missing energy $\not{E}_T$ and the transverse mass of the lepton plus missing energy system M_T^{ℓ}. It is clear that the backgrounds and the signal can be discriminated by $\not{E}_T$. Most events of the backgrounds are distributed in the region $\not{E}_T \lesssim 150$ GeV. However, the signal has much more events than backgrounds

in the region $\not{E}_T \gtrsim 150$ GeV, due to the extra missing energy from the massive LSP. Besides, the variable M_T^ℓ can well separate the backgrounds and signal because it has an end-point at the mass of the lepton's parent particle, $M_T^\ell|_{max} = M$ [66]. All the main backgrounds contain a W boson and a unique source of missing energy, the neutrino, coming from its decay. So the backgrounds have endpoint around M_W in the M_T^ℓ distributions. But the signal has a larger value of M_T^ℓ. A cut on $M_T^\ell \geq 80$ GeV will greatly reduce the backgrounds while keep most of the signal.

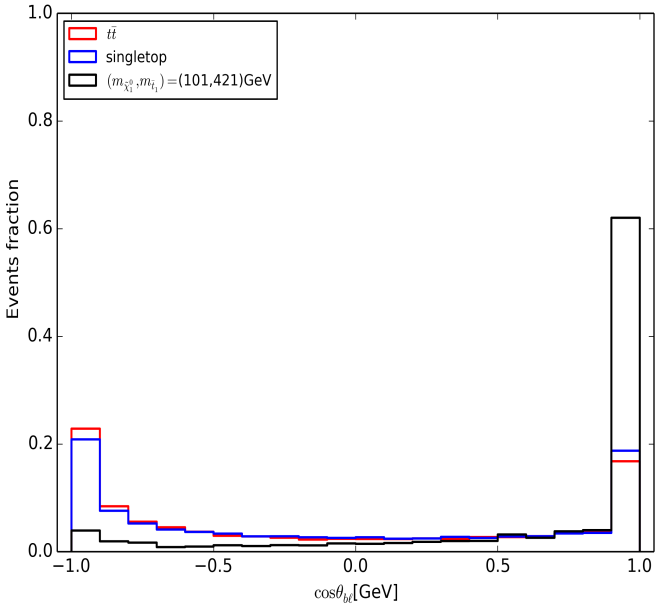

FIG. 4: Same as Fig. 3, but for the distribution of the opening angle $\cos\theta_{b\ell}$ between the charged lepton and the b-jet in the lab-frame.

Another interesting observable is the opening angle $\theta_{b\ell}$ between the charged lepton and the b-jet in the lab-frame. After requiring exactly one lepton and one b-jet, we display the distribution of $\cos\theta_{b\ell}$ in Fig. 4. We can see that most of the signal events fall in the region of $\cos\theta_{b\ell} > 0$, while the backgrounds have more events in the region of $\cos\theta_{b\ell} < 0$. This is because the the charged lepton and the b-quark from top quark in the stop decays are boosted so that they tend to move in the same direction when the mass splitting between $\tilde{t}_1$ and $\tilde{\chi}_1^0$ is large. Thus, the requirement of a large $\cos\theta_{b\ell}$ can further reduce backgrounds.

The detailed analysis strategies are the followings:

- We require exact one hard lepton with $p_T(\ell) > 30$ GeV and $|\eta_\ell| < 2.5$.

- We require exact one b-jet with $p_T(b) > 75$ GeV and $|\eta_b| < 2.5$ and veto extra jets with $p_T(j) > 20$ GeV to suppress the $t\bar{t}$ background.
- We define eight signal regions according to $\not{E}_T$ cuts: 150, 175, 195, 200, 205, 225, 250 and 275 GeV. It is worth noting at this point that cuts in M_T end up having little correlation with cuts in $\not{E}_T$, as it will be shown in the cut-flow tables below.
- We require $M_T^\ell > 175$ GeV and $\cos\theta_{b\ell} > 0.85$ to suppress top pair and single stop backgrounds.

Finally, we use the signal region with highest $S/\sqrt{B}$ to show our results in Fig. 5.

TABLE I: A cut flow analysis of the cross sections of the backgrounds and signal at 14 TeV LHC, where the cross sections are in unit of fb. The benchmark point is $(m_{\tilde{\chi}_1^0}, m_{\tilde{t}_1}) = (101, 421)$ GeV.

cut	1 lepton $p_T^\ell > 30GeV, \|\eta^\ell\| < 2.5$	1 b-jet $p_T^b > 75GeV, \|\eta^b\| < 2.5$	jet veto $p_T(j) > 20$GeV	$M_T^\ell > 175$ [GeV]	$\not{E}_T$ >150 [GeV]	$\cos\theta_{b\ell}$ >0.85
$t\bar{t}$	233465.16	77973.38	796.20	62.95	26.2472	11.75
$t + j/b/W$	44891.80	8411.10	189.24	9.45	3.47	1.64
signal	24.88	9.482	1.40	1.03	0.90	0.77
S/B(%)				1.43	3.02	5.75
$S/\sqrt{B}$				6.67	9.04	11.53

In Table I, we present a cut flow of cross sections for the signal and backgrounds at the 14 TeV LHC. The benchmark point is $m_{\tilde{\chi}_1^0} = 101$ GeV and $m_{\tilde{t}_1} = 421$ GeV. We can see that the $t\bar{t}$ production is the largest SM background. The requirement of exact one b-jet with $p_T^b > 75$ GeV can reduce the backgrounds by about 60%. The jet-veto for the second hard jet can significantly reduce the backgrounds by almost two orders of magnitude. The cuts of $M_T^\ell > 175$ GeV and $\not{E}_T > 150$ GeV can further remove the backgrounds by one order of magnitude. It should be noted that $\cos\theta_{b\ell} > 0.85$ can help to suppress backgrounds by 50% and improve the sensitivity S/B.

In Fig. 5, we plot the dependence of the signal significance $S/\sqrt{B}$ on $m_{\tilde{\chi}_1^0}$ and $m_{\tilde{t}_1}$ for the 14 TeV LHC with a luminosity $\mathcal{L} = 3000$ fb^{-1}. From this figure we can see that the significance drops with the increase of $m_{\tilde{\chi}_1^0}$ and $m_{\tilde{t}_1}$ because of the reduction of the cross section. We find that the parameter range 100 GeV $\leq m_{\tilde{\chi}_1^0} \leq 150$ GeV and $m_{\tilde{t}_1} \leq 760$ GeV

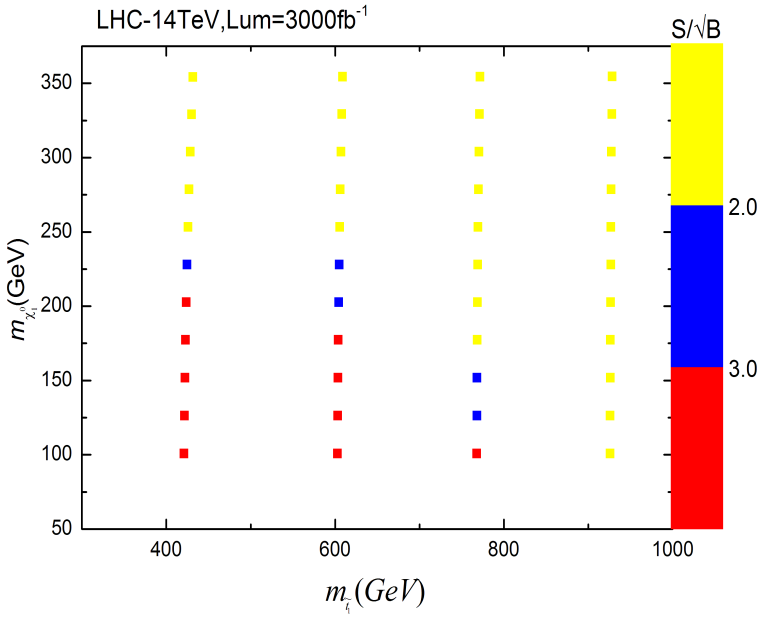

FIG. 5: The statistical significance $S/\sqrt{B}$ on the plane of $m_{\tilde{t}_1}$ versus $m_{\tilde{\chi}_1^0}$ for the 14 TeV LHC with $\mathcal{L} = 3000$ fb^{-1}.

can be covered at $\geq 2\sigma$ level with $S/B > 3\%$ at the HL-LHC, which is moderately better than the hadronic stop channel [42].

IV. CONCLUSION

In this work we explored the observability of the associated production of stop and chargino in the compressed electroweakino scenario at the 14 TeV LHC. Due to the small mass splitting between $\tilde{\chi}_1^0$ and $\tilde{\chi}_1^-$, such a production can lead to the mono-top signature via stop decay $\tilde{t}_1 \to t\tilde{\chi}_1^0$. We analyze the leptonic mono-top channel $pp \to \tilde{t}_1\tilde{\chi}_1^- \to b\ell + \not{E}_T$, and construct a lab-frame observable $\cos\theta_{b\ell}$ to reduce the SM backgrounds utilyzing the boosted top from the stop decay. We found that our single stop production can be probed at 2σ level at the 14 TeV LHC with $\mathcal{L} = 3000$ fb^{-1} when $m_{\tilde{t}_1} < 760$ GeV and $m_{\tilde{\chi}_1^0} < 150$ GeV.

ACKNOWLEDGMENTS

G. H. Duan thanks Yang Zhang for helpful discussions. This work is partly supported by the Australian Research Council, by the National Natural Science Foundation of China (NNSFC) under grants Nos. 11105124, 11105125, 11275057, 11305049, 11375001, 11405047, 11135003, 11275245, by the CAS Center for Excellence in Particle Physics (CCEPP) and by the CAS Key Research Program of Frontier Sciences.

[1] G. Aad *et al.* (ATLAS Collaboration), Phys. Lett. B **710**, 49 (2012).

[2] S. Chatrachyan *et al.* (CMS Collaboration), Phys. Lett. B **710**, 26 (2012).

[3] R. Barbieri and G. F. Giudice, Nucl. Phys. B **306**, 63 (1988).

[4] L. J. Hall, D. Pinner and J. T. Ruderman, JHEP **1204**, 131 (2012).

[5] M. Papucci, J. T. Ruderman and A. Weiler, JHEP **1209**, 035 (2012).

[6] C. Brust, A. Katz, S. Lawrence and R. Sundrum, JHEP **1203**, 103 (2012).

[7] J. Cao, C. Han, L. Wu, J. M. Yang and Y. Zhang, JHEP **1211**, 039 (2012) [arXiv:1206.3865 [hep-ph]].

[8] Z. Kang, T. Li, J. Li and Y. Liu, arXiv:1208.2673 [hep-ph].

[9] I. Low, Phys. Rev. D **88**, 095018 (2013).

[10] G. D. Kribs, A. Martin and A. Menon, Phys. Rev. D **88**, 035025 (2013).

[11] C. Han, K. Hikasa, L. Wu, J. M. Yang and Y. Zhang, JHEP **1310**, 216 (2013).

[12] K. Kowalska and E. M. Sessolo, Phys. Rev. D **88**, 075001 (2013).

[13] M. Backovic, A. Mariotti and M. Spannowsky, JHEP **1506**, 122 (2015) [arXiv:1504.00927 [hep-ph]].

[14] A. Kobakhidze, N. Liu, L. Wu and J. M. Yang, Phys. Rev. D **92**, 075008 (2015) [arXiv:1504.04390 [hep-ph]].

[15] B. Dutta *et al.*, Phys. Rev. D **90**, 095022 (2014).

[16] G. Belanger, D. Ghosh, R. Godbole and S. Kulkarni, JHEP **1509**, 214 (2015);

[17] A. Kobakhidze, N. Liu, L. Wu, J. M. Yang and M. Zhang, Phys. Lett. B **755**, 76 (2016).

[18] M. Drees and J. S. Kim, Phys. Rev. D **93**, 095005 (2016).

[19] H. Baer, V. Barger, M. Savoy and X. Tata, Phys. Rev. D **94**, 035025 (2016).

[20] J. Fan, R. Krall, D. Pinner, M. Reece and J. T. Ruderman, JHEP **1607**, 016 (2016) [arXiv:1512.05781 [hep-ph]].

[21] M. Schlaffer, M. Spannowsky and A. Weiler, Eur. Phys. J. C **76**, 457 (2016) [arXiv:1603.01638 [hep-ph]].

[22] D. Goncalves, K. Sakurai and M. Takeuchi, Phys. Rev. D **94**, 075009 (2016) [arXiv:1604.03938 [hep-ph]].

[23] D. Goncalves, K. Sakurai and M. Takeuchi, arXiv:1610.06179 [hep-ph].

[24]

[24] M. Aaboud *et al.* (ATLAS Collaboration), Phys. Rev. D **94**, 032005 (2016).

[25] The CMS collaboration, CMS-PAS-SUS-16-016.

[26] C. Han, J. Ren, L. Wu, J. M. Yang and M. Zhang, arXiv:1609.02361 [hep-ph].

[27] J. S. Kim, K. Rolbiecki, R. Ruiz, J. Tattersall and T. Weber, arXiv:1606.06738 [hep-ph].

[28] K. Kowalska, arXiv:1608.02489 [hep-ph].

[29] C. Han, M. M. Nojiri, M. Takeuchi and T. T. Yanagida, arXiv:1609.09303 [hep-ph].

[30] K. Kowalska and E. M. Sessolo, arXiv:1611.01852 [hep-ph].

[31] A. Barr and J. Liu, arXiv:1605.09502 [hep-ph].

[32] C. G. Lester and D. J. Summers, Phys. Lett. B **463**, 99 (1999) [hep-ph/9906349].

[33] A. Barr, C. Lester and P. Stephens, J. Phys. G **29**, 2343 (2003) [hep-ph/0304226].

[34] M. Drees, M. Hanussek and J. S. Kim, Phys. Rev. D **86**, 035024 (2012).

[35] Z. H. Yu, X. J. Bi, Q. S. Yan and P. F. Yin, Phys. Rev. D **87**, 055007 (2013).

[36] M. A. Ajaib, T. Li and Q. Shafi, Phys. Rev. D **85**, 055021 (2012).

[37] K. Hagiwara and T. Yamada, Phys. Rev. D **91**, 094007 (2015).

[38] H. An and L. T. Wang, Phys. Rev. Lett. **115**, 181602 (2015).

[39] S. Macaluso, M. Park, D. Shih and B. Tweedie, arXiv:1506.07885 [hep-ph].

[40] D. Goncalves, D. Lopez-Val, K. Mawatari and T. Plehn, Phys. Rev. D **90**, 075007 (2014);

[41] A. Ismail, R. Schwienhorst, J. S. Virzi and D. G. E. Walker, Phys. Rev. D **91**, 074002 (2015).

[42] K. Hikasa, J. Li, L. Wu and J. M. Yang, Phys. Rev. D **93**, 035003 (2016).

[43] N. Arkani-Hamed, A. Delgado and G. F. Giudice, Nucl. Phys. B **741**, 108 (2006).

[44] J. Andrea, B. Fuks and F. Maltoni, Phys. Rev. D **84**, 074025 (2011) [arXiv:1106.6199 [hep-ph]].

[45] J. Wang, C. S. Li, D. Y. Shao and H. Zhang, Phys. Rev. D **86**, 034008 (2012) [arXiv:1109.5963 [hep-ph]].

[46] J. L. Agram, J. Andrea, M. Buttignol, E. Conte and B. Fuks, Phys. Rev. D **89**, 014028 (2014) [arXiv:1311.6478 [hep-ph]].

[47] E. Alvarez, E. Coluccio Leskow, J. Drobnak and J. F. Kamenik, Phys. Rev. D **89**, 014016 (2014) [arXiv:1310.7600 [hep-ph]].

[48] I. Boucheneb, G. Cacciapaglia, A. Deandrea and B. Fuks, JHEP **1501**, 017 (2015) [arXiv:1407.7529 [hep-ph]].

[49] J. F. Gunion and H. E. Haber, Nucl. Phys. B **272**, 1 (1986).

[50] G. F. Giudice and A. Pomarol, Phys. Lett. B **372**, 253 (1996).

[51] C. Han, A. Kobakhidze, N. Liu, A. Saavedra, L. Wu and J. M. Yang, JHEP **1402**, 049 (2014).

[52] Z. Han, G. D. Kribs, A. Martin and A. Menon, Phys. Rev. D **89**, 075007 (2014);

[53] C. Han, D. Kim, S. Munir and M. Park, JHEP **1504**, 132 (2015);

[54] D. Barducci, *et al.*, arXiv:1504.02472 [hep-ph];

[55] J. Bramante, A. Delgado, F. Elahi, A. Martin and B. Ostdiek, Phys. Rev. D **90**, 095008 (2014);

[56] C. Han, L. Wu, J. M. Yang, M. Zhang and Y. Zhang, Phys. Rev. D **91**, 055030 (2015) [arXiv:1409.4533 [hep-ph]].

[57] A. Ismail, E. Izaguirre and B. Shuve, Phys. Rev. D **94**, 015001 (2016) [arXiv:1605.00658 [hep-ph]].

[58] A. Djouadi, J. -L. Kneur and G. Moultaka, Comput. Phys. Commun. **176**, 426 (2007).

[59] A. Djouadi, M. M. Muhlleitner and M. Spira, Acta Phys. Polon. B **38**, 635 (2007).

[60] J. Alwall *et al.*, JHEP **1407**, 079 (2014).

[61] R. D. Ball *et al.* [NNPDF Collaboration], Nucl. Phys. B **877**, 290 (2013).

[62] T. Sjostrand, S. Mrenna and P. Z. Skands, JHEP **0605**, 026 (2006).

[63] J. de Favereau *et al.* (DELPHES 3 Collaboration), JHEP **1402**, 057 (2014).

[64] M. Cacciari, G. P. Salam and G. Soyez, JHEP **0804**, 063 (2008).

[65] N. Kidonakis, Phys. Rev. D **84**, 011504 (2011).

[66] C. Patrignani *et al.* (Particle Data Group), Chin. Phys. C **40**, 100001 (2016).